

Detecting Anomalies in Systems for AI Using Hardware Telemetry

Ziji Chen

ziji.chen@eng.ox.ac.uk
University of Oxford

Peng Qian

peng.qian@eng.ox.ac.uk
University of Oxford

Steven W. D. Chien

steven.chien@eng.ox.ac.uk
University of Oxford

Noa Zilberman

noa.zilberman@eng.ox.ac.uk
University of Oxford

Abstract

Modern machine learning (ML) has grown into a tightly coupled, full-stack ecosystem that combines hardware, software, network, and applications. Many users rely on cloud providers for elastic, isolated, and cost-efficient resources. Unfortunately, these platforms as a service use virtualization, which means operators have little insight into the users' workloads. This hinders resource optimizations by the operator, which is essential to ensure cost efficiency and minimize execution time. In this paper, we argue that workload knowledge is unnecessary for system-level optimization. We propose Reveal, which takes a *hardware-centric* approach, relying only on hardware signals – fully accessible by operators. Using low-level signals collected from the system, Reveal detects anomalies through an unsupervised learning pipeline. The pipeline is developed by analyzing over 30 popular ML models on various hardware platforms, ensuring adaptability to emerging workloads and unknown deployment patterns. Using Reveal, we successfully identified both network and system configuration issues, accelerating the DeepSeek model by 5.97%.

1 Introduction

Modern machine learning (ML) workloads, especially deep neural networks (DNN) training, have shaped recent compute infrastructure. These workloads rely heavily on compute-intensive operations which requires specialized accelerators. Large language models (LLMs) such as ChatGPT [1], further push hardware limits [2]. The success of ML applications, such as in medical research [3], has further driven demand for deploying ML workloads. However, these devices are expensive; a single GPU costs tens of thousands of dollars [4], and together with the host system and maintenance, represents a considerable investment from cloud operators. This is demand for cloud-based AI resources is relentless, and is expected to grow 30% annually until 2030 [5].

Cloud operators provide users with environments to deploy ML applications using platform as a service (PaaS) [6, 7],

hiding the underlying hardware through virtualization. In this way, operators can satisfy users with different resource requirements, provide elasticity, reliability, and isolation.

While virtualization benefits cloud users, it leaves operators with limited workload knowledge. While important for privacy, security, and isolation, it is also problematic because modern ML application stacks have a tight hardware-software coupling. Individual components in the stack may be well optimized, but their integration is system- and workload-dependent. This is crucial, as small inefficiencies can cascade, leading to system-wide performance degradation and extended execution time. For example, distributed training relies heavily on collective communication, making the system prone to stragglers and network problems [8]. Even a minor power misconfiguration can cause up to $1.5\times$ slowdown [9], reducing performance and increasing operational costs.

Existing ML performance optimization works focus on a full-stack view [10–12]. It is difficult to diagnose performance anomalies without insights from the workload. Furthermore, what the user experiences inside a compute instance may differ from what happens on the hardware.

To tackle the lack of high-level observability, we argue that having a full-stack view is in fact *unnecessary* to detect system-level anomalies. Instead, we take a *hardware-centric* approach by considering only hardware-level metrics, which operators have full access to. We propose Reveal, a hardware-centric profiling and anomaly detection framework. Reveal is lightweight and collects hardware metrics using existing tools such as `perf` [13], widely available on Linux-based platforms. The framework is run on a bare-metal system by the operator, and sampled data is processed by an unsupervised anomaly detection pipeline. Reports are generated at intra- and inter-node levels, correlating anomalies across nodes.

The Reveal anomaly detection pipeline was developed by studying over 30 popular ML models, running on systems with different hardware characteristics. We identified a subset of hardware metrics that reflect the ML workload's behavior accurately. This design makes Reveal system- and workload-agnostic, supporting diverse hardware and both training and

inference. Using Reveal, we successfully identified five hardware configuration issues when running the DeepSeek model on an HPC cluster, accelerating end-to-end time by 5.97%.

In summary, we make the following contributions:

1. Introducing Reveal, a hardware-centric profiling and anomaly detection framework with high portability, deployability, and accurate analysis.
2. Identified a set of low-level performance metrics that are representative of ML workload’s behavior on hardware. We open-source all the collected datasets for future research.
3. Developed an unsupervised anomaly detection pipeline that detects performance problems running containerized ML workloads, successfully identifying system bottlenecks and accelerating DeepSeek by 5.97%.

2 Background and Motivation

ML workloads dominate modern data centers [5, 14], driving deployment of specialized accelerators and interconnects which are programmed via vendor libraries. ML frameworks such as Torch [15] and TensorFlow [16] further abstract them from training and inference logic. This creates a full-stack ecosystem, spanning from hardware, network, system software, and applications. Performance anomaly analysis for ML workload is especially challenging because of the tight coupling between layers. A long GPU kernel launch time could be due to launching overhead rather than GPU saturation, and a low GPU utilization is meaningless without correlating the application timeline [11]. Similarly, a slow input preprocessing pipeline could be a result of disk misconfiguration or inefficient caching, rather than a CPU processing bottleneck [10].

Existing works of ML profiling (Table 1) stress the importance of having full-stack information [17]. The Hotline profiler [12] complements profiling provided by frameworks, such as Torch [18], by merging and annotating their timeline with traces collected by other low-level runtimes, such as the CUDA profiling tool interface (cupti) and perf performance monitoring counters (PMCs). To improve coverage, RL-Scope [11] provides Python directives for developer to annotate critical paths in their code. Non-instrumentation tools such as Prometheus [19,20], and AWS SageMaker [21], do not modify applications. Instead, they sample operating system and hardware level statistics and perform anomaly analysis. Using these tools, ML developers can pinpoint where anomalies happen within a high-level workflow, specific functions, and attribute them to relevant hardware.

Lack of high-level observability. Despite the availability of analytic tools, most are designed for ML developers, rather than cloud system operators. Due to the isolation, the operator lacks high-level observability, rendering tools that require application integration or running inside instances inapplicable. Due to elasticity, how and when users deploy the application becomes unpredictable. Cloud users are free

to start, upscale, downscale, and stop their instances at any time. Workloads and scalability can also shift over time, for example, between training and inference dominance. This renders any one-size-fits-all configurations impractical. Our experiments (§6) revealed that misconfigured NIC interrupts could lead to GPU stalls, and unoptimized NVIDIA Collective Communications Library (NCCL) queue pair (QP) settings could lead to serialization. Both issues are detrimental to the performance of collective communication. Yet, without the perspective from the application, it is difficult to notice the issues.

Lack of insight. Existing profiling tools primarily *report* observations, rather than *analyze* them, leaving anomaly detection and diagnosis to performance engineers (Table 3). Furthermore, many have low coverage: framework profilers often cover the application and framework runtime, while tools like Plumber [10] only cover the input pipeline, making an overall assessment difficult. Rule-based triggers and supervised learning are widely used to identify anomalies, but come with severe limitations. Mycroft [8] is a profiling tool designed to improve collective communication. It is triggered using predefined thresholds, such as a throughput dropping by half. These thresholds often need workload-specific tuning and may be unsuitable for other subsystems. Thus, it is inapplicable to operators as they lack high-level visibility. Some anomaly detection methods use supervised learning [22], and require a ground truth to distinguish abnormal signals. eACGM [23] employs a Gaussian Mixture Model (GMM) for anomaly detection by training on recent data (e.g., the past hour). However, this method inherently assumes Gaussianity of the underlying distribution, an assumption often violated in practice, as system metrics are frequently skewed, heavy-tailed, and non-stationary. Moreover, ML workloads can run for extended periods, making the system susceptible to learning spurious or misleading signals. Both rule-based and supervised learning for anomaly detection are impractical for our use case, as system behavior is highly variable between workloads and deployments, reducing portability.

Overhead. Since operators deploy profiling and analysis on production systems, a low overhead is essential to avoid interfering with the applications. Unfortunately, many existing collection tools have high runtime and storage overhead. Plumber adds up to 21% for text workloads [10], while RL-Scope inflates GPU kernel launching time by up to 90.2% [11]. eBPF [26] offers lightweight, non-intrusive tracing from the kernel [23], but still give up to 17% runtime overhead [23, 27–30].

3 Reveal Architecture

We observe existing tools require high-level observability, lack adaptability, and impose high overhead – making them impractical for operators. Therefore, we propose Reveal, a profiling framework using unsupervised learning for auto-

Table 1: Comparison of monitoring & anomalies detection approaches.

Approach	Level	ML Code Instrum.	Subsystem Coverage	Anom. Det.	HW Attribution
TensorFlow [24] Profiler	App	Yes	CPU ^O (op time), GPU ^O (kernel timeline), Mem ^O (allocs)	No	No
PyTorch [18] Profiler	App	Yes	CPU ^O (op time), GPU ^O (kernel timeline), Mem ^O (allocs)	No	No
WandB [25]	App + Sys-Util	Yes	CPU ^S , GPU ^S , Mem ^S , Net ^S (coarse)	Rule-based	No
AWS SageMaker [21]	Sys-Util	No	CPU ^S , GPU ^S , Mem ^S , Disk ^S , Net ^S	Rule-based	Yes
Prometheus [19]	Sys-Util	No	CPU ^S , Mem ^S , Disk ^S , Net ^S ; GPU (partial)	Rule-based	No
Netdata	Sys-Util	No	CPU ^S , Mem ^S , Disk ^S , Net ^S ; GPU (partial)	ML-based	No
BCC / eBPF tools	Sys-Low	No	CPU ^K , Mem ^K , Disk ^K , Net ^K ; GPU (experimental)	No	Yes
RL-Scope [11]	App+Sys-Low	Yes	CPU ^{O+S} , GPU ^O , Mem ^O	Limited	Yes
Plumber [10]	Sys-Low	Yes	CPU ^I , Mem ^I , Disk ^I	Limited	Yes
eACGM [23]	Sys-Low	No	GPU ^S , Mem ^S , Net ^C , SW stack	ML-based	Yes
Reveal (This work)	Sys-Util + -Low	No	CPU ^{S+K} , GPU ^{S+K} , Mem ^{S+K} , Disk ^S , Net ^S	Yes	Yes

Level: App = application-level; Sys-Util = system utilization-level (coarse OS/infra metrics, e.g., CPU/GPU utilization, memory, I/O, network); Sys-Low = low-level tracing (kernel events, hardware counters). **Superscripts:** ^O = operator-level (framework ops/timeline); ^S = system-level (utilization counters, coarse metrics); ^K = kernel-level (syscalls, hardware counters); ^I = input pipeline (file read, buffer, prefetch); ^C = communication-level (NCCL / network communication). **ML Code Instrum.:** ML Code Instrumentation, whether ML training code requires modifications (profiler hooks/logging). **Subsystem Coverage:** Support for CPU, GPU, Mem (Memory), Disk (Storage), Net (Network), SW stack (Software stack); Op = Operator (framework operation, e.g., MatMul, Conv2D). **Anom. Det.:** Anomaly Detection, if the tool provides anomaly detection/alerting. *Limited* indicates the tool can highlight performance bottlenecks or misconfigurations, but not general-purpose anomaly detection or alerting. **HW Attribution:** Hardware Attribution, if anomalies are mapped to specific hardware subsystems.

matic anomaly analysis. As ML workloads are highly regular and repetitive [31], it is possible to capture relevant signals in the underlying hardware. Exploiting operators’ full access to bare-metal hardware, Reveal takes a *hardware-centric* approach, without requiring high-level observability.

Reveal collects data using existing lightweight tools, such as `perf` [13], and feeds them into an unsupervised anomaly detection pipeline for near-real-time node- and cluster-wide anomaly reports. Since collection is performed at the host level, we avoid redundant metrics; for example, cache misses are recorded once instead of once per container.

Container-level attribution can be achieved via Linux control groups (cgroups), exposing per-cgroup CPU, memory, and I/O statistics through a pseudo-filesystem. By correlating host counters with cgroup accounting, metrics can be remapped to individual containers. However, some challenges remain. Certain hardware events are not partitionable, `perf` and cgroup counters misalignment, cgroup v1/v2 differ in semantics, and elevated privileges requirements. Still, in operator-managed environments, these challenges are tractable. In summary, Reveal has the following design requirements:

High portability. Given the complexity of the cloud technology stack, Reveal must be highly portable, without coupling with any particular hardware, profiling tools, ML frameworks, job scheduling system, or being dependent on a specific kernel or OS. Reveal is also easily expandable to include new metrics, allowing it to adapt to new systems and accelerators.

Workload agnostic. Reveal supports diverse and unpredictable deployments, including training and inference, and across applications, such as computer vision (CV) and natural language processing (NLP). Furthermore, Reveal supports local and distributed workload, providing intra- and inter-node analysis. Since the operator has no visibility over the workload, the detection pipeline works even with an elastic workload, with unpredictable start/stop.

Analysis with precision. Reveal accurately detects anomalous

lies, identifying relevant subsystems, and attributing culprits, which could be manifested as other symptoms. It uses an unsupervised detection method, avoiding any rule-based threshold calibration.

Low overhead. Storage and compute overhead remain a challenge for traditional application profiling. Reveal uses the smallest number of metrics required to perform a detailed analysis. This ensures a low collection and analysis overhead, with minimal impact on the system.

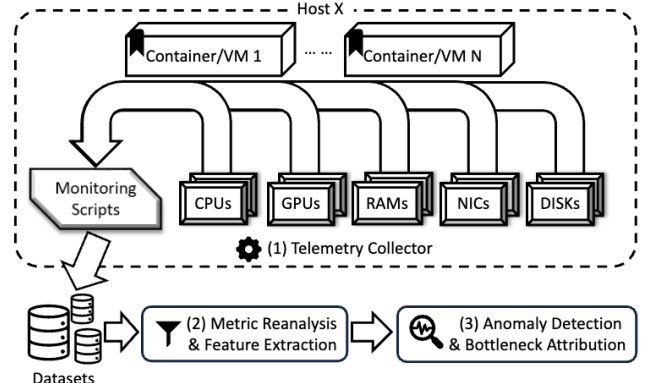


Figure 1: Host-level hardware anomaly analysis via Reveal.

3.1 Framework and Design

Reveal (Fig. 1) enables automatic data sampling and analysis with three main components: telemetry collector, metric reanalysis and extractor, and an anomaly detection engine.

Telemetry Collector. The Reveal prototype records approximately 150 unique metric types (which we draw from prior studies and best practices [21, 32]) per host using `perf` [13], `procfs` [33], `nvidia-smi` [34], and standard Linux utilities (Appendix A). The telemetry collector is flexible, where new probes (i.e., profiling tools) can be added. New metrics can be easily registered in its database to support novel hardware.

When replicated across CPU cores and GPUs, metrics collected by Reveal expand to over 700 time-series channels, while keeping CPU overhead below 1.5% (§5.3). In a data center-wide deployment with a high sampling rate, this can quickly overwhelm the storage requirements. Furthermore, having a large number of – not all relevant – metrics, could obscure automatic analysis. Therefore, Reveal only selects approximately 60% of them, significantly reducing storage overhead and simultaneously improving detection accuracy. We detail the filtering method in §4.1.

Metric Reanalysis and Feature Extraction. Certain raw signals are further transformed into derived metrics (Appendix B), such as IPC for execution throughput, branch misprediction rate for control flow irregularities, and cache miss or L3 stall ratios for memory hierarchy behavior. These derived indicators provide interpretable, low-level views of subsystem pressure and are computed in a lightweight post-processing step. Each time series is segmented into overlapping sliding windows, from which we extract a curated set of statistical features (e.g., moments, aggregate measures such as mean and variance) and temporal features (e.g., autocorrelation, linear trends) (§4.2). The resulting feature vectors capture both steady-state behavior and transient dynamics, enabling downstream anomaly analysis.

Anomaly Detection and Bottleneck Attribution Engine. Building on the resulting feature vectors, Reveal applies unsupervised detectors to detect anomaly occurrence and pinpoint where (§4.3). For each anomalous window, the engine highlights the implicated signals and attaches statistical or temporal explanations (§4.4). Anomalies are mapped to subsystem categories (CPU, GPU, memory, network, storage). To reduce false positives, the anomaly score increases with the number of detectors in agreement.

Reveal sometimes detects no anomalies within a time window. We regard the absence of anomalies as a valid outcome, indicating that the system is adequately provisioned and operating.

Reporting. Reports are adapted to deployment settings. In centralized infrastructures, where telemetry from many hosts can be aggregated, Reveal summarizes both per-host anomalies and cross-host imbalance. In decentralized settings, where each host processes data independently, reports remain local (though logs can later be consolidated into a shared database). The reporting pipeline supports both real-time alerts and periodic offline aggregation for retrospective diagnosis.

Preserving Evidence. Each automatically generated report retains raw anomaly evidence, including the anomalous window ID/timestamp, detection method, and the metric–feature pair that triggered the anomaly. An example report is provided in Appendix C. Figure 2 presents the anomaly detection results from three detectors, where hosts are not always flagged as anomalous at the same time.

Example. Figure 2 presents Reveal analyzing a DeepSeek

fine-tuning workload for text classification on a dual-host GPU setup. The results show that different detectors do not always flag anomalies at the same time across hosts.

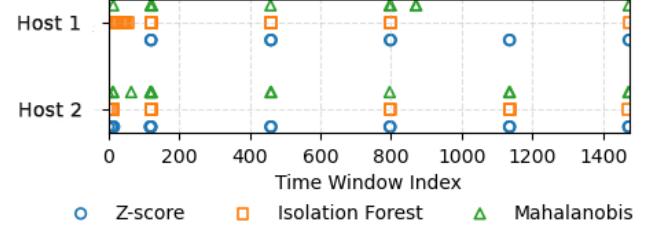


Figure 2: Anomalous windows detected by Reveal during DeepSeek fine-tuning on a dual-host GPU setup.

Figure 3 further demonstrates that a single anomalous window can exhibit *multiple distinct anomaly signals*, whose joint analysis enables root-cause attribution.

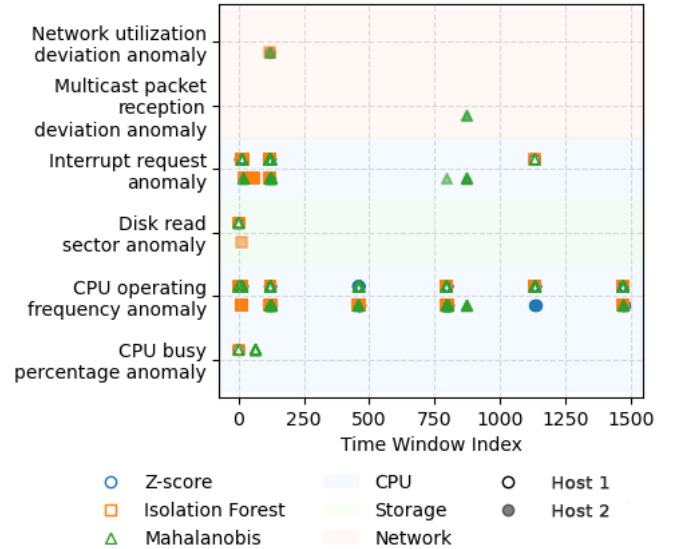


Figure 3: Causes of anomalous windows during DeepSeek fine-tuning on a dual-host GPU setup.

4 Anomaly Detection Pipeline

Having described the design goals and overall architecture of Reveal, the next question is how to select relevant metrics and design an accurate anomaly detection algorithm that attributes observations to root causes.

4.1 Metrics Selection

A central challenge in performance profiling lies in the sheer volume of data collected. Excess data can lead to information overload, often hindering rather than helping analysis. Many metrics are redundant in terms of diagnostic value. For example, at the microarchitectural level, *StallRatio* is strongly correlated with *OccupancyRatio*, *Cycle_activity_**,

and *Cache_Misses* (Pearson correlation coefficient $|r| \approx 0.81\text{--}0.998$). Similarly, storage-level counters such as *sectors_read*, *reads_completed_successfully*, and *reads_merged* show high correlations ($|r| \approx 0.86\text{--}0.97$). If Reveal were to sample all of them at a high rate, the resulting volume would quickly overwhelm both processing and storage, adding overhead without improving diagnostic value.

Given our focus on ML workloads, the key challenge is to identify *which metrics are most informative* and to understand *how indirect hardware signals expose characteristic differences across diverse ML workloads*. To understand the general behavior of ML applications on hardware, we perform a study on three systems in §5.2.

We evaluate more than 30 ML applications on systems equipped with GPUs or a CPU-only configuration (§5.2). The applications are selected to cover a wide range of workloads (e.g., NLP, CV), models (e.g., BERT [35]), and hardware requirements with different I/O, compute, and memory intensity. Details are described in § 5.1. We initially collect 150 metric types [21, 32]; their full specifications will be provided alongside the public dataset release.

We refine raw metrics using a correlation-driven pruning procedure. For each workload, we compute the average Pearson correlation matrix across all metrics. When a pair of metrics exceeds a global correlation threshold $|r|$, we retain one as representative and mark the other as redundant.

As shown in Figure 4, the *Avg Multi-R²* proxy (yellow) measures how well each metric can be linearly predicted from the remaining ones (via regression). It remains saturated until the threshold falls below $|r| = 0.5$, indicating that the retained set still preserves the full linear information. The *Avg Max|r|* (blue) represents each metric’s strongest correlation with any other metric in the set; its value is still above 0.8 at $|r| = 0.5$, meaning pruning at this point removes only strongly redundant signals. The *Selected Ratio* (green) reflects set size rather than information content; at $|r| = 0.5$, roughly 40% of time-series channels are removed.

Taken together, the curves reveal an inflection near $|r| = 0.5$, where pruning removes substantial redundancy yet retains the majority of useful diagnostic information. So we adopt $|r| = 0.5$ as a conservative pruning threshold here.

Within each cluster, we select a single metric using a deterministic ranking scheme: (1) *a fixed priority table* that favors interpretable utilization and throughput counters (e.g., CPU utilization, GPU utilization, memory usage, network throughput, disk I/O); and (2) *variance-based tie-breaking*, retain more informative metrics with higher correlation variance.

To ensure workload-agnostic applicability, we merge pruning results across a diverse set of ML workloads and take the union of all retained metrics. This union defines the final diagnostic space used in Reveal.

Diagnostic Coverage of Retained Metrics. Even after pruning, the retained metrics span all major subsystems and cap-

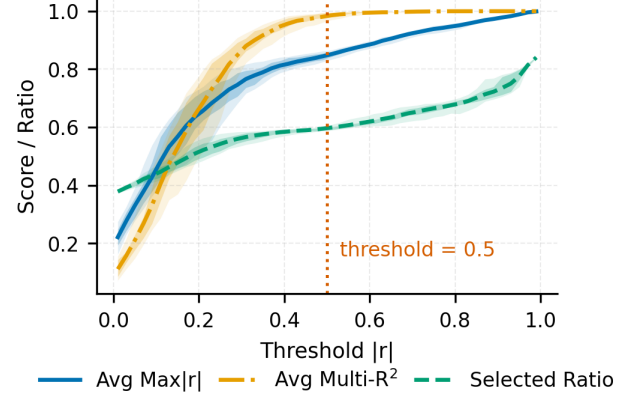


Figure 4: Effect of correlation threshold $|r|$ on pruning. Pruning at $|r| = 0.5$ removes substantial redundancy while preserving most diagnostic information.

ture the dominant failure modes in ML workloads. These signals map to known inefficiencies, as outlined below:

CPU. Utilization, Busy%, idle-state residency (C6), core/package frequencies, interrupts (IRQ/SMI), and power counters reveal imbalance, preemption, firmware events, and DVFS/thermal throttling, while PMU metrics such as IPC, stall ratios, cache usage, branch prediction, memory access latency, and hardware lock elision events expose microarchitectural back-pressure, locality issues, and contention.

GPU. Utilization (core/memory), memory usage, clock/power/thermal sensors, PCIe link width, and ECC/retired-page counters highlight starvation, throttling, and reliability faults.

Memory. Utilization, dirty/writeback pages, swap usage, huge pages, and error counters capture allocator fragmentation, leaks, and out-of-memory risks.

Network. Rx/Tx throughput, error/drop/retransmission counters, and protocol/connection statistics diagnose collective communication imbalance and transport inefficiencies.

Storage. Sector operations, I/O queue depth, merge patterns, and service times reveal I/O stalls and pipeline bottlenecks.

Together, this curated set provides host-visible coverage of accelerator starvation, thermal throttling, memory pressure, network loss/retransmission, storage stalls, and reliability events, enabling timely anomaly detection without application instrumentation.

4.2 Sliding Window Feature Extraction

Raw monitoring streams are noisy and highly autocorrelated, making individual samples poor indicators of workload state. By default, Reveal collects metrics at 100 ms intervals (configurable). To capture short-term trends and reduce noise, we segment each metric’s time series into overlapping windows (3 s, 1 s stride) and extract temporal features from each window. Rather than treating each raw sample as independent, this approach captures temporal dynamics that are critical

for distinguishing anomalies and bottlenecks from benign fluctuations.

Within each window, metrics fall into three categories: (1) *Dynamic signals* (e.g., utilization, throughput, stall counters), for which we compute statistical and temporal features such as moments, linear trends, autocorrelation, and stationarity tests; (2) *Error or event counters* (e.g., ECC errors, page faults, retransmissions), which are aggregated by summation to capture burstiness; (3) *Static or strictly periodic metrics* (e.g., buffer size, thermal sensors, power states), which provide little intra-host variation and are excluded in single-host anomaly detection, but remain in cross-host deviations (e.g., thermal imbalance) anomaly detection.

Reveal annotates each window with statistical and temporal features, capturing anomalies that point-in-time statistics or coarse-grained profiling would miss.

4.3 Unsupervised Anomaly Detection

To detect anomalies in system-level telemetry without labels, we employ three complementary methods: Z-score, Mahalanobis distance in a principal component analysis (PCA) subspace, and Isolation Forest. Together, they capture single-metric spikes and joint departures across metrics while remaining lightweight and interpretable. We adopt conservative thresholds widely used in prior work, typically flagging the top 1% [36].

We choose these detectors for four reasons: (1) compatibility with unlabeled telemetry, (2) robustness to noise, (3) interpretability for operators, and (4) modest computational cost. Prior systems research and Artificial Intelligence for IT Operations (AIOps) studies have shown that such methods are both practical and scalable for real-time anomaly detection [37, 38]. AIOps introduced unsupervised learning techniques into production-scale operations, analyzing service logs and application-level metrics to automatically detect system failures. Similarly, our telemetry cannot be easily labeled: beyond intentionally injected faults, manual anomaly annotation is both unconvincing and prohibitively expensive, as it requires exhaustive trace analysis. This further motivates the use of unsupervised detectors in our setting.

Z-score. A lightweight statistical baseline [39] that flags outliers via standardized deviations from a window’s workload-specific distribution. We flag windows exceeding the 99th percentile of the mean absolute Z-score. Its simplicity and alignment with the “three-sigma” rule make it suitable for low-noise metrics and first-pass alerting.

Mahalanobis distance in a PCA subspace. Features are first projected onto principal components that retain 95% variance, then each window’s Mahalanobis distance to the workload centroid is computed as the anomaly score. Windows above the 99th percentile are marked. Unlike Euclidean distance, Mahalanobis accounts for correlations and scale differences across metrics, making it effective at detecting

anomalies that only occur in joint patterns. PCA has long been effective for isolating faults from high-dimensional telemetry and logs [40, 41].

Isolation Forest (IF). A tree-based ensemble method [42] that recursively partitions data to isolate rare points; the average path length yields an isolation score. We train an IF per workload with a 1% contamination rate. IF scales well, handles skewed or multimodal distributions, and is robust to transient noise; it is widely deployed (e.g., Amazon CloudWatch streaming anomaly detection) [43–45].

Each detector evaluates every window for anomalies, and the results are used both for reporting and for assessing cross-detector agreement. Taken together, the trio identifies threshold-like violations, correlated multivariate shifts, and broader distributional outliers, without supervision or handset thresholds. By combining agreement across complementary detectors, Reveal reduces false positives from any single method while preserving sensitivity to diverse anomaly types.

4.4 Bottleneck Attribution and Interpretation

For each detected anomaly window, Reveal maps anomalies back to their originating time-series signals and records temporal explanations (e.g., mean shifts, abnormal trends, variance spikes). This enables fine-grained attribution across CPU, GPU, memory, network, and storage subsystems.

A single anomaly window often involves multiple correlated signals rather than a single failing metric. In such cases, anomalies are attributed jointly across subsystems. For example, a window may simultaneously show variance shifts in CPU Busy%, skewed IRQ distributions, and irregular disk read activity (*sectors_read*). Such co-occurrence reveals interactions across components, such as interrupt imbalance coinciding with I/O bursts, providing stronger evidence of anomalies than any single metric independently. In distributed ML workloads, anomalies are further localized to specific nodes or hosts, enabling operators to identify not only which subsystem is stressed but also where in the cluster.

Across ML workloads, we observe recurring categories of bottlenecks: *CPU imbalance and stalls* (Busy% saturation, IRQ spikes, L3 stall ratios); *Memory pressure* (dirty/writeback surges, swap activity); *GPU contention* (memory exhaustion, PCIe down-training, thermal throttling); *Network anomalies* (TCP retransmission bursts, packet drops); *Storage delays* (long I/O queue times, irregular merge patterns). Several categories align with prior diagnosis literature [46, 47], confirming that the surfaced signals reflect bottleneck behaviors.

Rather than claiming a single “root cause,” Reveal aids diagnosis by automatically attributing anomalies to subsystems and highlighting their main contributors, enabling engineers to prioritize deeper investigation. Its goal is not transient fault recovery or online remediation, but the identification of persistent and meaningful bottlenecks, although the same reports can still be surfaced in real time for alerting.

5 Evaluation

5.1 ML Workloads

We evaluate Reveal on a diverse suite of ML applications spanning NLP and CV tasks. Specifically, we run **26 applications** on a GPU-equipped HPC cluster and **23 applications** on a CPU-only local cluster using the same software stack.

The applications cover both training and inference across multiple model families, including Bidirectional Encoder Representations from Transformers (BERT) [35], Bidirectional and Auto-Regressive Transformers (BART) [48], Residual Neural Networks (ResNet) [49], Vision Transformers (ViT) [50], Visual Geometry Group networks (VGG) [51], DeepSeek-R1 Distill-Qwen (DeepSeek) [52], Large Language Model Meta AI (LLaMA) [53], and Mistral [54]. The workloads include text classification, table question answering, image classification, and semantic segmentation, using standardized training and inference pipelines.

All models are trained on public datasets, including General Language Understanding Evaluation/SST2 (GLUE/SST2) [55], WikiSQL [56], PASCAL Visual Object Classes (PASCAL VOC) [57], Canadian Institute for Advanced Research (CIFAR) [58], and Modified National Institute of Standards and Technology dataset (MNIST) [59], using consistent batch sizes, optimizers, and training epochs across tasks.

We choose these workloads because they are representative in research and actively used according to our surveys [60–64]. Furthermore, they are covered in recognized benchmarks [65], enabling comparison. These models stress the system differently. For example, CNN/Transformer requires sustained compute and memory bandwidth; LLM serving/training is communication and memory bound; whereas recommendation systems are I/O bound. They thoroughly examine Reveal’s detection capability across subsystems.

To support constrained CPU-only environments, we include compact LLM variants (1B LLaMA [53], 1.5B DeepSeek [52]) for CPU-only clusters, and apply quantized LoRA fine-tuning across all LLMs. Appendix E provides a complete mapping of applications, models, datasets, and tasks.

5.2 Experimental Setup

We evaluate Reveal on the following systems, and Appendix D lists software versions and dependencies.

HPC Cluster: We collect data from two GPU environments. The first is an HPC system equipped with two NVIDIA Tesla V100 GPUs (32 GB variant) and an Intel Xeon Platinum 8628 CPU (48 cores). They have 384 GB of host memory and are connected via InfiniBand HDR100. We allocate two nodes. The second is a single-node HPC system equipped with four NVIDIA H100 GPUs, with 96 GB HBM3. The host uses a recent Intel Sapphire Rapids CPU (48 cores @ 2.0 GHz) with

1.5 TB of system memory. We run the ML workloads inside Apptainer containers with a Conda environment (PyTorch 2.6.0, CUDA 12.4, RAPIDS). Host-level telemetry is recorded throughout execution.

Local Cluster We use a local cluster to evaluate the CPU-only environment. Our local cluster consists of nine servers, each equipped with a single AMD EPYC 7443P CPU (24 cores). We enable hyperthreading to use 48 threads. The system has 256 GB system memory, and 8 GB swap, connected via a 100 GE Tofino Ethernet switch. We run 11 Apptainer containers per node, with each allocating four threads and 20 GB memory, resulting in a 99-container distributed training setup. We use the identical software stack as in the HPC systems.

5.3 Overhead and Efficiency

Before showing Reveal’s effectiveness in diagnosing anomalies, we evaluate its overhead to ensure it is suitable for production deployment.

Monitoring Overhead. Figure 5 reports CPU overhead across different sampling intervals of Reveal (100–600 ms), compared against `perf stat` at 100 ms. We observe that Reveal overhead decreases as the sampling interval increases: from $\sim 1.2\text{--}1.4\%$ at 100 ms to below 0.6% at 600 ms. At 200–300 ms, Reveal already matches or falls below the overhead of `perf stat`. While Reveal introduces slightly higher cost at aggressive sampling (100 ms), its overhead remains under 2% across all settings and becomes negligible at moderate intervals, making it practical for continuous deployment.

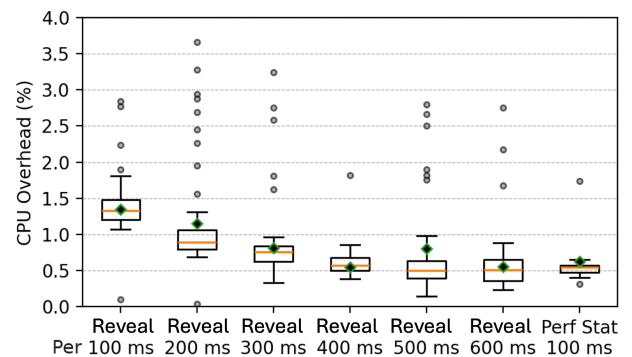


Figure 5: CPU overhead of Reveal at different sampling frequencies, compared with `perf stat` at 100 ms.

Storage Requirements. Each host generates approximately 42–43 KB/s of telemetry when collecting ~ 700 time series channels (prototype) at a 100 ms sampling interval. This represents a worst-case scenario in which all raw signals are retained, resulting in ~ 3.6 GB/day per node. After filtering, we typically retain ~ 400 metrics, lowering the footprint to 14–22 KB/s ($\sim 1.2\text{--}1.9$ GB/day per host), which is manageable in practice. Further reductions are achievable by adjusting the sampling interval (e.g., 200 ms) or applying lightweight

compression (e.g., gzip, lz4). For long-running deployments, standard retention policies—such as per-epoch summarization or rolling windows—can further control storage costs without sacrificing anomaly detection fidelity.

Detector Runtime Efficiency. We profile both feature extraction and anomaly detectors. Feature extraction takes 1.46 ± 0.02 s per 3 s window, with Parquet materialization at 0.667 ± 0.005 s, yielding an end-to-end latency of 2.26 ± 0.17 s. Among detectors, the Z-score method is extremely lightweight at 0.0011 ± 0.0003 s, Mahalanobis distance in a PCA subspace adds 0.015 ± 0.020 s, while Isolation Forest dominates the runtime when enabled, averaging 0.08 ± 0.07 s. Overall, feature extraction, distance computation, and anomaly scoring complete within seconds, making the framework lightweight and well-suited for online batch processing or periodic profiling in production environments.

5.4 Robustness of System Metrics

Our retained metrics reflect workload dynamics and behaviors rather than environmental noise or measurement artifacts. For each metric, we compute its Dynamic Time Warping (DTW) distance between all runs and a median trace. Across 99.75% of workload–metric pairs, we observe statistically significant similarity (p-values < 0.05 from a two-sided Wilcoxon signed-rank test), indicating that system behavior under controlled conditions is highly reproducible.

5.5 Impact of Window Granularity

Sliding-window configuration directly impacts anomaly resolution and noise sensitivity. We study the effect of sliding-window size/stride on anomaly detection. Reveal’s default setting uses 3 s/1 s; we compare with finer (1.5 s/0.5 s) and coarser (5 s/2 s) settings.

Agreement Measures. We quantify cross-configuration agreement using a length-based Intersection-over-Union (IoU) over merged anomaly intervals. Let I_A and I_B be two sets of merged anomaly intervals, and let $L(\cdot)$ denote total covered length. With interval intersection length $L(I_A \cap I_B)$,

$$\text{IoU}(I_A, I_B) = \frac{L(I_A \cap I_B)}{L(I_A) + L(I_B) - L(I_A \cap I_B)}.$$

We also report two hit-rate metrics: (i) *byCount*, the fraction of anomaly segments in A that intersect any segment in B ; and (ii) *byLength*, the fraction of anomaly length in A overlapping B . These complement IoU by being less sensitive to small boundary jitters.

Findings. Across ML applications on the HPC cluster, baseline vs. fine-grained slicing shows stable concurrence (hit-rate *byCount* mean 0.92, median 1.0) despite boundary shifts that lower IoU (median 0.50). Coarse slicing maintains aggregate overlap (IoU median 0.53, hit-rate *byCount* 0.78) but smooths short anomalies. Direct fine–coarse comparison yields the

weakest agreement (IoU 0.39, *byCount* 0.68), confirming that extreme settings diverge most (Table 2, Fig. 6).

Table 2: Hit-rate agreement across window settings.

Pair (size/stride)	Hit <i>byCount</i>			Hit <i>byLength</i>		
	mean	median	std	mean	median	std
Default vs. 1.5 s/0.5 s	0.92	1.00	0.14	0.72	0.74	0.15
Default vs. 5 s/2 s	0.75	0.78	0.23	0.72	0.74	0.23
1.5 s/0.5 s vs. 5 s/2 s	0.67	0.68	0.21	0.66	0.67	0.21

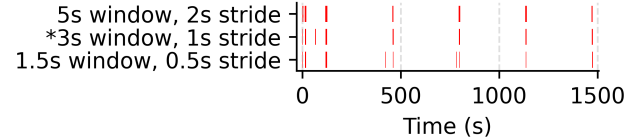


Figure 6: Effect of window granularity on anomaly timelines.

5.6 Results

Reveal detects anomalies invisible to conventional metrics and attributes them to low-level signals across CPU, memory, network, and storage. Together, they reveal many anomalies from cross-subsystem interactions. For example, I/O bursts triggering CPU frequency scaling, concentrated interrupts driving coordinated CPU oscillations, or network retransmissions propagating into GPU stalls. Beyond anomaly detection, Reveal’s host-level telemetry exposes heterogeneous utilization patterns across applications.

Anomaly Patterns.

On the HPC clusters, GPUs drive the bulk of vector computation, while other subsystems sustain the data flow and support tasks. We observe that slowdowns often originate in supporting components, most notably the CPU, rather than the GPU. Reveal shows that CPU-side signals (*Bzy_MHz*, *IRQ*) dominate, contributing over 50% of the features selected in anomalous windows. DeepSeek fine-tuning runs report average over 540 seconds of anomalous *Bzy_MHz* and nearly 300 seconds of *IRQ* spikes, together accounting for approximately 14.26% of all detected anomalies. Memory-residency anomalies (*Unevictable*, *Writeback*) and I/O stalls (*sectors_read*, *writes_merged*) recur, indicating inefficiencies in the data pipeline. Across all ML applications, we observe recurrent TCP retransmissions. By mapping raw metrics, we find that a portion of these retransmissions reflects NCCL-level imbalance. This effect is particularly pronounced in models such as Mistral and ViT-L16.

On the local cluster, anomalies concentrate in the memory and I/O subsystems. For image-classification runs (e.g., VGG16/19, ResNet50), we repeatedly observe multi–tens-of-seconds episodes of memory writeback and dirty-page buildup. We further observe TCP retransmissions and receive

drops, with their cumulative stall time exceeding 100 seconds per run. These results suggest significant contention in I/O queues and within the network stack. Unlike the HPC cluster, the local cluster reveals anomalies in low-level performance counters (e.g., `ls_dispatch`, `dc_accesses`), exposing pipeline stalls invisible to coarse-grained profiling.

Across all evaluated applications, anomalies can be broken down by subsystem as follows: **CPU**. IRQ imbalance and CPU utilization oscillations are widespread, often coinciding with I/O bursts. **Memory**. The local cluster exhibits writeback surges and dirty-page buildup, whereas the HPC cluster shows non-reclaimable page anomalies indicative of NUMA residency imbalance. **Network**. TCP retransmissions arise in both environments: they are often associated with NCCL imbalance in distributed GPU training, and kernel-level queue drops in CPU inference when analyzed jointly with co-occurring anomalies. **Storage**. Across workloads (e.g., DeepSeek, ResNet), short-lived bursts in read/write activity point to transient congestion along the storage path.

Root Cause Analysis (RCA).

Single anomaly window often reveals concurrent issues spanning multiple subsystems. We illustrate how Reveal facilitates root cause reasoning with two micro-examples.

Micro-example 1: Storage bursts. Reveal detects on Host 2 concurrent anomalies in window 13, shown in Fig. 3, for storage reads (`sectors_read kurtosis`) and CPU frequency (`Bzy_MHz variance`). Their temporal alignment reflects I/O bursts triggering scheduling overheads, which prompt the governor to adjust `Bzy_MHz`, making storage activity the likely root cause.

Micro-example 2: Interrupt pressure. Reveal detects on Host 1 `Bzy_MHz` shifts with bursts of `IRQ` features across CPU threads, shown in windows 120–122 of Fig. 3. This indicates interrupt pressure driving coordinated frequency fluctuations, amplified by unbalanced IRQ distribution.

Together, these examples show how Reveal links cross-subsystem anomalies to actionable root causes.

6 Case Studies

In this section, we present five case studies where Reveal successfully identified anomalies and their root causes, and report the results of rectifying the problems. Anomaly detection, node, and subsystem attribution are automatic. Runtime remediation is not possible for most kinds of anomalies; therefore, we assume manual remediation. Figures and analysis are provided to explain the problems.

NUMA anomalies (Memory).

Detection. In the same dual-host GPU setup running DeepSeek-7B fine-tuning, Reveal flagged anomalies clustered around windows 118–123 (see Fig. 2). The corresponding raw traces (Fig. 7) reveal a sharp drop in instructions per cycle

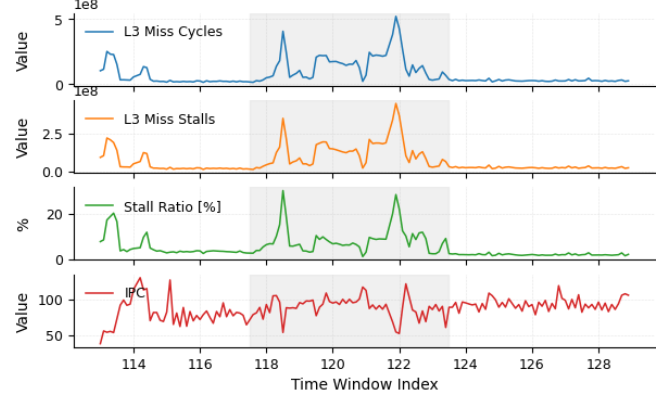


Figure 7: Raw traces under NUMA misplacement. Windows 118–123 show IPC drops with increased L3 miss cycles, L3 miss stalls, and stall ratio.

(IPC) together with pronounced increases in L3 miss cycles, L3 miss stalls, and stall ratio, indicating memory inefficiency.

Analysis. The co-occurrence of IPC degradation and stall spikes is consistent with cross-socket memory and PCIe traffic: when CPU execution and memory allocation are not NUMA-local to the GPU, requests traverse inter-socket interconnect, increasing latency and reducing effective bandwidth. This leads to elevated L3 miss penalties and stall cycles.

Remediation. We modified the launch script to pin each training process to a single NUMA node, binding both its CPU set and memory allocation to the NUMA domain collocated with its GPU and InfiniBand NIC. This configuration avoids cross-NUMA memory and PCIe accesses while preserving proximity to the communication path.

Impact. With NUMA-aware binding, anomalies related to memory stalls and network inefficiency became less frequent. InterStat-labeled anomalies decreased from 3.82% to 1.17%, and TCP-retransmission anomalies dropped from 3.51% to 2.94%. Busy%-variance anomalies increased moderately (6.91% → 10.44%), reflecting that tighter CPU binding concentrates load on fewer cores. The end-to-end runtime of the DeepSeek-7B fine-tuning workload improved from 1823.4 ± 46.1 s to 1714.6 ± 70.0 s (*mean* ± approx. 95% CI), corresponding to a relative reduction of 5.97%. Training LLMs with large datasets (e.g. on one trillion tokens) often takes weeks on large GPU clusters [66]. Even for 7B-parameter models, fine-tuning may take tens of hours on modern single-GPU hardware [67]. Thus, a 6% reduction in runtime translates into substantial total time savings in real-world large-scale training.

NCCL-QPs misconfiguration (Network).

Detection. In the same dual-host GPU setup running DeepSeek-7B fine-tuning, Reveal also flagged anomalies clustered around windows 64–66 (see Fig. 2). The corresponding raw traces (Fig. 8) reveal a step increase in CPU Busy%,

synchronized bursts in `ib0` TX/RX throughput, and an unexpected flattening of TCP retransmissions, while GPU power draw declines as the devices wait for data.

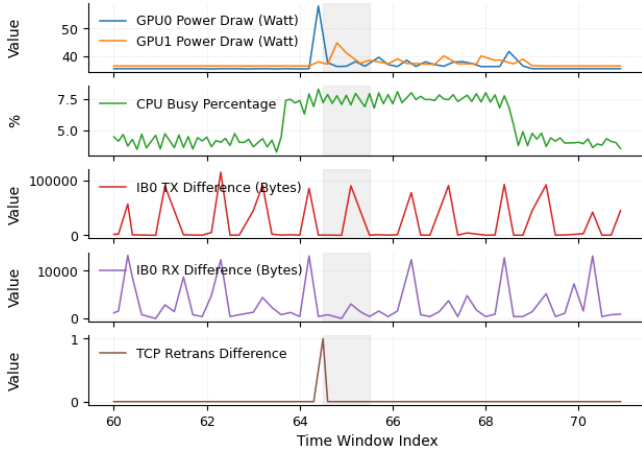


Figure 8: Raw traces under Single-QP communication. In windows 64–66, CPU Busy% increases, `ib0` TX/RX traffic becomes bursty, and TCP retransmissions spike, while GPU power remains flat.

Analysis. The increase in CPU Busy% alongside bursty `ib0` traffic, without a corresponding rise in retransmissions, indicates that the bottleneck lies not in link bandwidth but in the completion handling path. With a single QP/CQ configuration, all completion events are funneled through a limited set of interrupt vectors, concentrating handling on a few cores. This creates softirq backlog and head-of-line blocking, amplifying completion latency and ultimately manifesting as stalled GPU data supply and reduced power draw.

Remediation. We reconfigured NCCL to allocate multiple QPs per connection, increasing from 1QP to 2QP. This change parallelizes send/receive and completion processing, spreading interrupts across more vectors and cores. It requires no application-level modifications and is transparent to the training framework.

Impact. Switching from 1QP to 2QP reduced the incidence of Busy%- and TCP-retransmission-labeled anomalies by 59% and 73%, respectively, while IRQ-labeled anomalies increased from 37.9% to 46.5%. Storage-related anomalies showed a slight decrease, and CPU-frequency (Bzy_MHz) anomalies remained largely unchanged. The marked reduction in retransmission anomalies highlights a healthier communication path: fewer stalls, smoother GPU data supply, and more predictable network behavior. In large-scale deployments, such improvements in infrastructure health are as critical as direct performance gains, as they mitigate cascading slowdowns and reduce operational risk. At the same time, the end-to-end runtime of the DeepSeek-7B fine-tuning workload was 1825.4 ± 46.1 s with 1QP and 1769.3 ± 16.7 s with 2QPs, corresponding to a relative reduction of 3.1%.

IRQ imbalance (CPU).

Detection. In a dual-host GPU setup running DeepSeek-7B fine-tuning, Reveal flagged co-occurring anomalies in CPU Busy% variance and IRQ counters, forming multiple clusters of anomalous windows (Fig. 2, e.g., windows 1115–1118).

Analysis. The co-occurrence of Busy% spikes and IRQ bursts indicates that NIC and storage interrupts were concentrated on a small subset of cores, creating hotspots. This imbalance likely slowed down communication by creating softirq backlog, stalling GPU kernels while waiting for data [68].

Remediation. We compared configurations with and without the `irqbalance` service. The NVIDIA `mlx5` driver raises many IRQs (one per completion queue plus asynchronous IRQs), making manual per-IRQ pinning complex and error-prone. In contrast, enabling `irqbalance` automatically spreads interrupt load across more cores.

Impact. With `irqbalance` enabled, the probability of anomaly windows linked to single-core Busy% decreased (from $8.20\% \pm 2.90\%$ to $6.91\% \pm 2.11\%$), and anomalies raised by TCP-retransmission also dropped (from 6.07% to 3.51%). In contrast, the overall IRQ-labeled share remained nearly unchanged ($\sim 0.5\%$), showing that `irqbalance` redistributes rather than reduces interrupts. End-to-end runtime did not significantly improve, consistent with `irqbalance` making generic rather than workload-specific decisions. Nevertheless, the reduction in retransmission anomalies indicates smoother packet processing and suggests that more deliberate strategies (e.g., NUMA-aware manual IRQ placement) could yield tangible runtime gains.

HugePages misconfiguration (Memory).

Detection. In a 9-host CPU-only setup running all evaluated workloads, one of the nodes persistently exhibited abnormally higher memory usage across all test workloads (see Figure 9). This anomaly was surfaced by Reveal’s cross-node analysis on memory counters, which highlighted the node deviating from the cluster baseline.

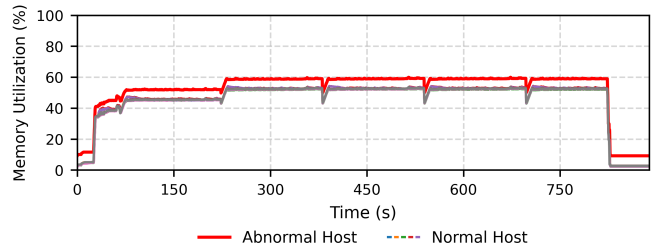


Figure 9: Memory utilization anomaly across the hosts. One host persistently consumed more memory than the others.

Analysis. Deeper inspection revealed that the anomalous node had preallocated 1 GiB HugePages. These pages were unused by applications but reported as “used” memory by the OS, creating the illusion of a heavily loaded node. Such misconfigurations are subtle: conventional utilization dashboards would simply report high memory pressure without distinguishing

between allocated but idle HugePages and truly used ones.

Remediation. We reconfigured the affected node to use the default 2 MiB HugePages allocation, consistent with the other eight hosts, instead of preallocating 1 GiB HugePages. This fix required no application changes and immediately corrected the memory usage report.

Impact. Reported memory usage normalized, eliminating the false imbalance across the cluster and preventing misleading monitoring results. More broadly, this case underscores that Reveal can separate benign configuration artifacts from genuine workload stress. By surfacing the misconfiguration at the system level, Reveal avoided potential misdiagnoses that could have led operators to incorrectly attribute performance issues to memory exhaustion or to mistakenly reschedule workloads across the cluster.

Injected Packet Loss (Network).

Background. Packet loss is a well-known cause of performance degradation, often manifesting as training slowdowns in distributed workloads. It frequently stems from network congestion, leading to TCP retransmits, or faulty links [69]. Since TCP retransmits are unavoidable in production clusters, we injected controlled loss rates (0.1/0.2/1%) into a dual-host GPU setup to systematically study their impact.

Detection. Already before injecting loss, Reveal detects that large-scale training, fine-tuning and inference workloads naturally generate retransmissions due to their bursty, high-volume traffic. LLM inference workloads exhibit only sparse spikes (tens of retransmissions per run), whereas LLM fine-tuning produces thousands of retransmissions with frequent, model-specific bursts. With loss injected, Reveal consistently flagged *network-related* counters among the top-1% anomalies. This is despite the injected loss not inflating retransmission counts by orders of magnitude compared to the baseline, nor changing average throughput; instead, the anomaly *patterns* shifted. At 0.1% loss, retransmissions became more bursty and temporally aligned with NIC-utilization jitter. At 0.2% loss, anomalies expanded to protocol-level fluctuations (e.g., connection churn). At 1% loss, retransmission spikes co-occurred with CPU IRQ variance and *Bzy_MHz* oscillations.

Analysis. Given injected loss, retransmissions observed by Reveal fell into two distinct categories. (1) *Workload-intrinsic retransmissions* (2) *Fault-induced retransmissions*: in practice, these would be caused by congestion or link faults, but here they are emulated by the injected loss. Traditional monitoring only reports “retransmissions” without distinguishing between these two categories. In contrast, Reveal contextualizes retransmissions: when they co-occur with cross-subsystem effects (e.g., IRQ imbalance and GPU stalls), they are classified as *fault-induced*; when confined to workload traffic patterns, they are identified as *workload-intrinsic*.

Impact. Reveal’s ability to distinguish between inherent workload behavior and loss caused by faults or congestion is important in production clusters, where operators need to react

and fix the second type of losses. This is a significant advantage over traditional monitoring systems, which typically report retransmission counts only as coarse statistics. As these systems cannot attribute retransmissions to specific causes, operators often treat them as noisy signals: acknowledged but not acted upon. Prior studies confirm that retransmissions are non-negligible in large-scale traces yet frequently overlooked in performance analyses [70]. Even current cloud services (e.g., AWS CloudWatch) expose retransmission metrics without cross-layer attribution [43], leaving operators uncertain about whether remediation is necessary.

Reveal’s ability to analyze retransmissions spans across subsystems: from transport-level counters to CPU IRQ surges and GPU stalls. By providing this cross-layer context, Reveal elevates retransmissions from “mere noise” to actionable indicators of infrastructure health, allowing operators to make informed decisions about when intervention is required.

7 Discussion

Generality Across Platforms. Reveal generalizes across both diverse computing architectures and hardware generations. Although our evaluation primarily targets x86-64 CPUs and NVIDIA GPUs, the selected system-level metrics have equivalent counterparts across other platforms (§3, §4.1), including Intel, AMD, ARM, and RISC-V. Since Reveal works with raw telemetry without architecture-specific assumptions, it is portable across hardware. Despite the generational gap between A100 and H100 GPUs, Reveal captured anomaly patterns effectively without extra tuning. Although anomalies and bottlenecks manifest differently across hardware generations and accelerators, e.g., SM utilization or memory bandwidth saturation on GPUs, these signals remain semantically equivalent at the subsystem level. Since Reveal maps counters into subsystems, it ensures applicability across platforms.

Implementation Portability. Beyond hardware diversity, a natural question is the portability of the implementation. Over 91% of Reveal’s codebase is reusable without modification when ported to new architectures. The monitoring, metric filtering, and anomaly detection modules are entirely portable, while only a thin layer (fewer than 20 lines) must be adapted to interface with platform-specific telemetry backends (e.g., perf on x86, pmu-tools on ARM). In practice, this adaptation requires only a few engineer-hours, making Reveal lightweight to deploy across heterogeneous platforms.

Operational Implications. Beyond improving anomaly detection accuracy, the feature selection pipeline provides actionable benefits for system operators. By systematically identifying stable, discriminative, and non-redundant signals, Reveal reduces the monitoring footprint from hundreds of raw counters to a manageable subset. This enables performance and infrastructure engineers to prioritize metrics that directly reflect resource bottlenecks, improving observability while minimizing monitoring overhead.

Table 3: Comparison of bottleneck analysis research methodologies.

Approach	Analysis Targets	Method Type	Data Source	Granularity	Automation	Attribution
AWS [71]	Comm. overhead	Rule-based heuristics	Comm + profiler logs	Job	Manual	Device, link
Meta [72]	GPUs comm. cost	Profiling + stats	Runtime + hw logs	Job	Manual	Topology
MIT [73]	Network demands	Topology-aware	Net + sched logs	Job, Sub-job	Semi-automatic	Topology
Microsoft [74, 75]	HBM R/W mismatch	Analytical model	HBM metrics	Subsystem	Manual	Mem. access pattern
Google (Plumber) [10]	Input-pipeline stalls, op bottlenecks	Top-down op analysis	Op-level stats + util., subsystem util.	Operator	Automatic	Pipeline + host res.
Alibaba [76]	Storage burstiness	Quantile + I/O analysis	Storage + infra logs	Time window	Semi-automatic	I/O
Hu et al. [7]	GPU idle from IO stalls	Trace + log correlation	Infra logs	Job	Manual	Cross-layer
Reveal (Our work)	Host-level RCA	Timeline corr.	GPU + I/O stats	Event	Manual	GPU/Upstream latency
		Unsupervised ML	Host-level telemetry (CPU/GPU/Mem/Net/Disk)	Time window	Fully automatic	Subsystems

Abbreviations: Comm. = Communication, Stat. = Statistical, Hw = Hardware, Acc. = Accelerator, Net. = Network, R/W = Read/Write, Op = Operator, Util. = Utilization, Sched. = Scheduler, R/W = Read/Write, Res. = Resources, Infra = Infrastructure, Corr. = Correlation, RCA = Root Cause Analysis.

Limitations and Future Work. Our current pipeline uses fixed sampling rates and static window sizes, which prevents it from adapting to workload dynamics. However, this is not a fundamental problem. Heuristic-based methods (e.g., adjusting frequency after a stable period) are trivial to implement in Reveal. While Reveal pinpoint anomalies accurately, it cannot resolve them without operator intervention. We plan to investigate lightweight runtime interventions, which can be automatically triggered by Reveal. For example, an IRQ imbalance could trigger affinity rebalancing automatically.

8 Related Work

Performance bottlenecks in current ML systems span all subsystems. AWS [71] and Meta [72] reported communication accounting for 12–44% of training time, varying across workloads and accelerators, with optimized collectives yielding $1.9\times$ speedup. Cassini [73] showed significant network performance variance across workloads on the same setup.

Storage and memory bottlenecks are also well-documented. Microsoft [74] finds HBM to be overprovisioned for writes yet underperforming under read-heavy access. Google [10, 78, 79] emphasizes full-stack profiling for fault tolerance and systemic bottlenecks. Alibaba [76] highlights storage burstiness driven by concurrent CPU, memory, and network stress. Hu et al. [7] observe GPU underutilization in LLM workloads due to I/O stalls and scheduler delays. At cloud scale, MLaaS systems exhibit long-tail latency and cross-layer contention [77, 80], challenging root-cause diagnosis.

By combining multi-subsystem telemetry with unsupervised anomaly detection, Reveal reliably identifies anomalies that prior studies have recognized as critical, such as I/O stalls and memory bandwidth saturation, for which existing tools

are often intrusive, narrow in scope, or unsuitable for continuous deployment. It also detects inefficiencies that have received less attention in the literature, e.g., CPU frequency oscillations, interrupt imbalance, deferred writeback and dirty-page buildup. Reveal complements prior work by enabling efficient and fine-grained detection of both well-known and previously underexplored inefficiencies. These insights arise from high-resolution, multi-metric time-series analysis, rather than utilization-only or trace-based profiling. Tables 1 and 3 provide detailed comparisons with production monitoring systems and recent research efforts.

9 Conclusion

Lack of high-level visibility is a major obstacle to performance optimization by operators. In this paper, we introduced Reveal to overcome the visibility problem, using only low-level metrics. Our anomaly detection pipeline combines three unsupervised methods and turns noisy raw measurements into actionable insights about workload behavior. Unlike existing work, Reveal is highly portable and deployable, without coupling to any application or systems. Reveal moves bottleneck detection from one-off profiling sessions to a continuous, data-driven process, and points toward a future where ML infrastructure can not only identify problems but adapt to them in real time. We see this as a step towards building an efficient ML system. The dataset collected and Reveal will be open-sourced to enable further research by the community.

For the purpose of Open Access, the author has applied a CC BY public copyright license to any Author Accepted Manuscript version arising from this submission.

References

[1] Tom Brown, Benjamin Mann, Nick Ryder, Melanie Subbiah, Jared D Kaplan, Prafulla Dhariwal, Arvind Neelakantan, Pranav Shyam, Girish Sastry, Amanda Askell, et al. Language models are few-shot learners. *Advances in neural information processing systems*, 33:1877–1901, 2020.

[2] Jared Kaplan, Sam McCandlish, Tom Henighan, Tom B Brown, Benjamin Chess, Rewon Child, Scott Gray, Alec Radford, Jeffrey Wu, and Dario Amodei. Scaling laws for neural language models. *arXiv preprint arXiv:2001.08361*, 2020.

[3] Vera Sorin, Eyal Klang, Miri Sklair-Levy, Israel Cohen, Douglas B Zippel, Nora Balint Lahat, Eli Konen, and Yiftach Barash. Large language model (chatgpt) as a support tool for breast tumor board. *NPJ Breast Cancer*, 9(1):44, 2023.

[4] Ben Cottier, Robi Rahman, Loredana Fattorini, Nestor Maslej, Tamay Besiroglu, and David Owen. The rising costs of training frontier ai models, 2025.

[5] Akamai. Ai in cloud computing: How is ai revolutionizing the landscape, 2025. Accessed: April 4, 2025.

[6] HPCwire News. MLPerf v5.0 Reflects the Shift Toward Reasoning in AI Inference. <https://www.hpcwire.com/2025/04/02/mlperf-v5-0-reflects-the-shift-toward-reasoning-in-ai-inference/>, Apr 2025.

[7] Qinghao Hu, Zhisheng Ye, Zerui Wang, Guoteng Wang, Meng Zhang, Qiaoling Chen, Peng Sun, Dahua Lin, Xiaolin Wang, Yingwei Luo, Yonggang Wen, and Tianwei Zhang. Characterization of large language model development in the datacenter, 2024.

[8] Yangtao Deng, Lei Zhang, Qinlong Wang, Xiaoyun Zhi, Xinlei Zhang, Zhuo Jiang, Haohan Xu, Lei Wang, Zuquan Song, Gaohong Liu, et al. Mycroft: Tracing dependencies in collective communication towards reliable llm training. *arXiv preprint arXiv:2509.03018*, 2025.

[9] Prasoon Sinha, Akhil Guliani, Rutwik Jain, Brandon Tran, Matthew D Sinclair, and Shivaram Venkataraman. Not all gpus are created equal: characterizing variability in large-scale, accelerator-rich systems. In *SC22: International Conference for High Performance Computing, Networking, Storage and Analysis*, pages 01–15. IEEE, 2022.

[10] Michael Kuchnik, Ana Klimovic, Jiri Simsa, Virginia Smith, and George Amvrosiadis. Plumber: Diagnosing and removing performance bottlenecks in machine learning data pipelines. *Proceedings of Machine Learning and Systems*, 4:33–51, 2022.

[11] James Gleeson, Moshe Gabel, Gennady Pekhimenko, Eyal de Lara, Srivatsan Krishnan, and Vijay Janapa Reddi. Rl-scope: Cross-stack profiling for deep reinforcement learning workloads. *Proceedings of Machine Learning and Systems*, 3:783–799, 2021.

[12] Daniel Snider, Fanny Chevalier, and Gennady Pekhimenko. Hotline profiler: Automatic annotation and a multi-scale timeline for visualizing time-use in dnn training. In D. Song, M. Carbin, and T. Chen, editors, *Proceedings of Machine Learning and Systems*, volume 5, pages 104–126. Curran, 2023.

[13] perf — linux performance analysis tools. <https://perfwiki.github.io/main/>. Accessed May 2025.

[14] Zhisheng Ye, Wei Gao, Qinghao Hu, Peng Sun, Xiaolin Wang, Yingwei Luo, Tianwei Zhang, and Yonggang Wen. Deep learning workload scheduling in gpu data-centers: A survey. *ACM Computing Surveys*, 56(6):1–38, 2024.

[15] Adam Paszke, Sam Gross, Francisco Massa, Adam Lerer, James Bradbury, Gregory Chanan, Trevor Killeen, Zeming Lin, Natalia Gimelshein, Luca Antiga, et al. Pytorch: An imperative style, high-performance deep learning library. *Advances in neural information processing systems*, 32, 2019.

[16] Martín Abadi, Paul Barham, Jianmin Chen, Zhifeng Chen, Andy Davis, Jeffrey Dean, Matthieu Devin, Sanjay Ghemawat, Geoffrey Irving, Michael Isard, et al. {TensorFlow}: a system for {Large-Scale} machine learning. In *12th USENIX symposium on operating systems design and implementation (OSDI 16)*, pages 265–283, 2016.

[17] Rajveer Bachkaniwala, Harshith Lanka, Kexin Rong, and Ada Gavrilovska. Lotus: Characterization of machine learning preprocessing pipelines via framework and hardware profiling. In *2024 IEEE International Symposium on Workload Characterization (IISWC)*, pages 30–43, 2024.

[18] PyTorch Team. Pytorch profiler: Performance debugging for pytorch programs, 2021. Accessed: April 4, 2025.

[19] James Turnbull. *Monitoring with Prometheus*. Turnbull Press, 2018.

[20] Google Cloud Platform. Managed Service for Prometheus. <https://cloud.google.com/managed-prometheus>, Sep 2025.

[21] Ameet V. Joshi. *Amazon’s Machine Learning Toolkit: Sagemaker*, pages 233–243. Springer International Publishing, Cham, 2020.

[22] Chuanhao Sun, Ujjwal Pawar, Molham Khoja, Xenofon Foukas, Mahesh K. Marina, and Bozidar Radunovic. Spotlight: Accurate, explainable and efficient anomaly detection for open ran. In *Proceedings of the 30th Annual International Conference on Mobile Computing and Networking*, ACM MobiCom ’24, page 923–937, New York, NY, USA, 2024. Association for Computing Machinery.

[23] Ruilin Xu, Zongxuan Xie, and Pengfei Chen. eacgm: Non-instrumented performance tracing and anomaly detection towards machine learning systems, 2025.

[24] Google. Tensorboard: Visualizing learning, 2023. Accessed: April 4, 2025.

[25] Weights and Biases. Weights & biases, 2018. Software available from wandb.com.

[26] Bolaji Gbadamosi, Luigi Leonardi, Tobias Pulls, Toke Høiland-Jørgensen, Simone Ferlin-Reiter, Simo Sorce, and Anna Brunström. The ebpf runtime in the linux kernel, 2024.

[27] Li-Der Chou, Luo-You Jian, and Yan-Wen Chen. ebpf-based network monitoring platform on kubernetes. In *2024 6th International Conference on Computer Communication and the Internet (ICCCI)*, pages 140–144, 2024.

[28] Marcelo Abranches, Oliver Michel, Eric Keller, and Stefan Schmid. Efficient network monitoring applications in the kernel with ebpf and xdp. In *2021 IEEE Conference on Network Function Virtualization and Software Defined Networks (NFV-SDN)*, pages 28–34, 2021.

[29] Mathieu Jadin, Quentin De Coninck, Louis Navarre, Michael Schapira, and Olivier Bonaventure. Leveraging ebpf to make tcp path-aware. *IEEE Transactions on Network and Service Management*, 19(3):2827–2838, 2022.

[30] Sepehr Abbasi Zadeh, Ali Munir, Mahmoud Mohamed Bahnasy, Shiva Ketabi, and Yashar Ganjali. On augmenting tcp/ip stack via ebpf. In *Proceedings of the 1st Workshop on EBPF and Kernel Extensions*, eBPF ’23, page 15–20, New York, NY, USA, 2023. Association for Computing Machinery.

[31] Steve Rhyner, Haocong Luo, Juan Gómez-Luna, Mhammad Sadrosadati, Jiawei Jiang, Ataberk Olgun, Harshita Gupta, Ce Zhang, and Onur Mutlu. Pim-opt: Demystifying distributed optimization algorithms on a real-world processing-in-memory system, 2024.

[32] Yu Gan, Mingyu Liang, Sundar Dev, David Lo, and Christina Delimitrou. Sage: practical and scalable ml-driven performance debugging in microservices. In *Proceedings of the 26th ACM International Conference on Architectural Support for Programming Languages and Operating Systems*, ASPLOS ’21, page 135–151, New York, NY, USA, 2021. Association for Computing Machinery.

[33] /proc — process information pseudo filesystem. <https://man7.org/linux/man-pages/man5/proc.5.htm>. Accessed May 2025.

[34] Nvidia system management interface (nvidia-smi). <https://developer.nvidia.com/system-management-interface>. Accessed May 2025.

[35] Jacob Devlin, Ming-Wei Chang, Kenton Lee, and Kristina Toutanova. Bert: Pre-training of deep bidirectional transformers for language understanding, 2019.

[36] Muhammad Imran. Development of machine-learning based app for anomaly detection in CMSWEB. Technical report, CERN, Geneva, 2025.

[37] Peter Bodik, Moises Goldszmidt, Armando Fox, Dawn B. Woodard, and Hans Andersen. Fingerprinting the datacenter: automated classification of performance crises. In *Proceedings of the 5th European Conference on Computer Systems*, EuroSys ’10, page 111–124, New York, NY, USA, 2010. Association for Computing Machinery.

[38] Xu Zhang, Qingwei Lin, Yong Xu, Si Qin, Hongyu Zhang, Bo Qiao, Yingnong Dang, Xinheng Yang, Qian Cheng, Murali Chintalapati, Youjiang Wu, Ken Hsieh, Kaixin Sui, Xin Meng, Yaohai Xu, Wenchi Zhang, Furao Shen, and Dongmei Zhang. Cross-dataset time series anomaly detection for cloud systems. In *2019 USENIX Annual Technical Conference (USENIX ATC 19)*, pages 1063–1076, Renton, WA, July 2019. USENIX Association.

[39] GitLab Observability Team. Using prometheus for anomaly detection. <https://about.gitlab.com/blog/2019/03/27/prometheus-metrics-and-alerts/>, 2019. Accessed May 2025.

[40] Anukool Lakhina, Mark Crovella, and Christophe Diot. Diagnosing network-wide traffic anomalies. In *Proceedings of the 2004 Conference on Applications, Technologies, Architectures, and Protocols for Computer Communications*, SIGCOMM ’04, page 219–230, New York, NY, USA, 2004. Association for Computing Machinery.

[41] Wei Xu, Ling Huang, Armando Fox, David Patterson, and Michael I. Jordan. Detecting large-scale system

problems by mining console logs. In *Proceedings of the ACM SIGOPS 22nd Symposium on Operating Systems Principles, SOSP '09*, page 117–132, New York, NY, USA, 2009. Association for Computing Machinery.

[42] Fei Tony Liu, Kai Ming Ting, and Zhi-Hua Zhou. Isolation forest. In *2008 Eighth IEEE International Conference on Data Mining*, pages 413–422, 2008.

[43] Amazon cloudwatch anomaly detection. https://docs.aws.amazon.com/AmazonCloudWatch/latest/monitoring/CloudWatch_Anomaly_Detection.html, 2024. Accessed May 2025.

[44] Deepika Marella, Roopa Navya Muthi, Buchammagari Avinash Reddy, Kaniganti Priyanka Saraswathi, Vijender Busi Reddy, and Nenavath Srinivas Naik. Unveiling network anomalies: A comparative study of real-time log-based detection approach. In *2023 IEEE 20th India Council International Conference (INDICON)*, pages 1216–1221, 2023.

[45] Scalable anomaly detection for observability data. <https://www.eyer.ai/blog/scalable-anomaly-detection-algorithms-for-observability/>, 2023. Accessed May 2025.

[46] Eli Cortez, Anand Bonde, Alexandre Muzio, Mark Russinovich, Marcus Fontoura, and Ricardo Bianchini. Resource central: Understanding and predicting workloads for improved resource management in large cloud platforms. In *Proceedings of the International Symposium on Operating Systems Principles (SOSP)*, October 2017.

[47] Liana V. Rodriguez, Alexis Gonzalez, Pratik Poudel, Raju Rangaswami, and Jason Liu. Unifying the data center caching layer: feasible? profitable? In *Proceedings of the 13th ACM Workshop on Hot Topics in Storage and File Systems, HotStorage '21*, page 50–57, New York, NY, USA, 2021. Association for Computing Machinery.

[48] Mike Lewis, Yinhan Liu, Naman Goyal, Marjan Ghazvininejad, Abdelrahman Mohamed, Omer Levy, Ves Stoyanov, and Luke Zettlemoyer. Bart: Denoising sequence-to-sequence pre-training for natural language generation, translation, and comprehension, 2019.

[49] Kaiming He, Xiangyu Zhang, Shaoqing Ren, and Jian Sun. Deep residual learning for image recognition, 2015.

[50] Alexey Dosovitskiy, Lucas Beyer, Alexander Kolesnikov, Dirk Weissenborn, Xiaohua Zhai, Thomas Unterthiner, Mostafa Dehghani, Matthias Minderer, Georg Heigold, Sylvain Gelly, Jakob Uszkoreit, and Neil Houlsby. An image is worth 16x16 words: Transformers for image recognition at scale, 2021.

[51] Karen Simonyan and Andrew Zisserman. Very deep convolutional networks for large-scale image recognition, 2015.

[52] DeepSeek-AI. Deepseek-r1: Incentivizing reasoning capability in llms via reinforcement learning, 2025.

[53] Hugo Touvron, Thibaut Lavril, Gautier Izacard, Xavier Martinet, Marie-Anne Lachaux, Timothée Lacroix, Baptiste Rozière, Naman Goyal, Eric Hambro, Faisal Azhar, Aurelien Rodriguez, Armand Joulin, Edouard Grave, and Guillaume Lample. Llama: Open and efficient foundation language models, 2023.

[54] Albert Q. Jiang, Alexandre Sablayrolles, Arthur Mensch, Chris Bamford, Devendra Singh Chaplot, Diego de las Casas, Florian Bressand, Gianna Lengyel, Guillaume Lample, Lucile Saulnier, Lélio Renard Lavaud, Marie-Anne Lachaux, Pierre Stock, Teven Le Scao, Thibaut Lavril, Thomas Wang, Timothée Lacroix, and William El Sayed. Mistral 7b, 2023.

[55] Alex Wang, Amanpreet Singh, Julian Michael, Felix Hill, Omer Levy, and Samuel R. Bowman. Glue: A multi-task benchmark and analysis platform for natural language understanding, 2019.

[56] Victor Zhong, Caiming Xiong, and Richard Socher. Seq2sql: Generating structured queries from natural language using reinforcement learning, 2017.

[57] Mark Everingham, S. M. Eslami, Luc Gool, Christopher K. Williams, John Winn, and Andrew Zisserman. The pascal visual object classes challenge: A retrospective. *Int. J. Comput. Vision*, 111(1):98–136, January 2015.

[58] Alex Krizhevsky. Learning multiple layers of features from tiny images. *University of Toronto*, 05 2012.

[59] Y. Lecun, L. Bottou, Y. Bengio, and P. Haffner. Gradient-based learning applied to document recognition. *Proceedings of the IEEE*, 86(11):2278–2324, 1998.

[60] Jun Bi, Qi Guo, Xiaqing Li, Yongwei Zhao, Yuanbo Wen, Yuxuan Guo, Enshuai Zhou, Xing Hu, Zidong Du, Ling Li, Huaping Chen, and Tianshi Chen. Heron: Automatically constrained high-performance library generation for deep learning accelerators. In *Proceedings of the 28th ACM International Conference on Architectural Support for Programming Languages and Operating Systems, Volume 3, ASPLOS 2023*, page 314–328, New York, NY, USA, 2023. Association for Computing Machinery.

[61] Qinghao Hu, Meng Zhang, Peng Sun, Yonggang Wen, and Tianwei Zhang. Lucid: A non-intrusive, scalable and interpretable scheduler for deep learning training

jobs. In *Proceedings of the 28th ACM International Conference on Architectural Support for Programming Languages and Operating Systems, Volume 2*, ASPLOS 2023, page 457–472, New York, NY, USA, 2023. Association for Computing Machinery.

[62] Diandian Gu, Yihao Zhao, Yinmin Zhong, Yifan Xiong, Zhenhua Han, Peng Cheng, Fan Yang, Gang Huang, Xin Jin, and Xuanzhe Liu. Elasticflow: An elastic serverless training platform for distributed deep learning. In *Proceedings of the 28th ACM International Conference on Architectural Support for Programming Languages and Operating Systems, Volume 2*, ASPLOS 2023, page 266–280, New York, NY, USA, 2023. Association for Computing Machinery.

[63] Cong Guo, Jiaming Tang, Weiming Hu, Jingwen Leng, Chen Zhang, Fan Yang, Yunxin Liu, Minyi Guo, and Yuhao Zhu. Olive: Accelerating large language models via hardware-friendly outlier-victim pair quantization. In *Proceedings of the 50th Annual International Symposium on Computer Architecture*, ISCA ’23, page 1–15. ACM, June 2023.

[64] Yining Shi, Zhi Yang, Jilong Xue, Lingxiao Ma, Yuqing Xia, Ziming Miao, Yuxiao Guo, Fan Yang, and Lidong Zhou. Welder: Scheduling deep learning memory access via tile-graph. In *17th USENIX Symposium on Operating Systems Design and Implementation (OSDI 23)*, pages 701–718, Boston, MA, July 2023. USENIX Association.

[65] Vijay Janapa Reddi, Christine Cheng, David Kanter, Peter Mattson, Guenther Schmuelling, Carole-Jean Wu, Brian Anderson, Maximilien Breughe, Mark Charlebois, William Chou, Ramesh Chukka, Cody Coleman, Sam Davis, Pan Deng, Greg Diamos, Jared Duke, Dave Fick, J. Scott Gardner, Itay Hubara, Sachin Idgunji, Thomas B. Jablin, Jeff Jiao, Tom St. John, Pankaj Kanwar, David Lee, Jeffery Liao, Anton Lokhmotov, Francisco Massa, Peng Meng, Paulius Micikevicius, Colin Osborne, Gennady Pekhimenko, Arun Tejasve Raghunath Rajan, Dilip Sequeira, Ashish Sirasao, Fei Sun, Hanlin Tang, Michael Thomson, Frank Wei, Ephrem Wu, Lingjie Xu, Koichi Yamada, Bing Yu, George Yuan, Aaron Zhong, Peizhao Zhang, and Yuchen Zhou. Mlperf inference benchmark, 2020.

[66] Ziheng Jiang, Haibin Lin, Yinmin Zhong, Qi Huang, Yangrui Chen, Zhi Zhang, Yanghua Peng, Xiang Li, Cong Xie, Shibiao Nong, Yulu Jia, Sun He, Hongmin Chen, Zhihao Bai, Qi Hou, Shipeng Yan, Ding Zhou, Yiyao Sheng, Zhuo Jiang, Haohan Xu, Haoran Wei, Zhang Zhang, Pengfei Nie, Leqi Zou, Sida Zhao, Liang Xiang, Zherui Liu, Zhe Li, Xiaoying Jia, Jianxi Ye, Xin Jin, and Xin Liu. Megascale: Scaling large language model training to more than 10,000 gpus, 2024.

[67] Ashvini Kumar Jindal, Pawan Kumar Rajpoot, and Ankur Parikh. Birbal: An efficient 7b instruct-model fine-tuned with curated datasets, 2024.

[68] Michael LeBeane, Khaled Hamidouche, Brad Benton, Mauricio Breternitz, Steven K. Reinhardt, and Lizy K. John. Gpu triggered networking for intra-kernel communications. In *Proceedings of the International Conference for High Performance Computing, Networking, Storage and Analysis*, SC ’17, New York, NY, USA, 2017. Association for Computing Machinery.

[69] Erez Weintraub, Ron Banner, and Ariel Orda. Distributed training under packet loss, 2025.

[70] Kostas Pentikousis, Hussein Badr, and Asha Andrade. A comparative study of aggregate tcp retransmission rates. *International Journal of Computers and Applications*, 32(4), 2010.

[71] Jun Huang, Zhen Zhang, Shuai Zheng, Feng Qin, and Yida Wang. DISTMM: Accelerating distributed multi-modal model training. In *21st USENIX Symposium on Networked Systems Design and Implementation (NSDI 24)*, pages 1157–1171, Santa Clara, CA, April 2024. USENIX Association.

[72] Liang Luo, Buyun Zhang, Michael Tsang, Yinbin Ma, Ching-Hsiang Chu, Yuxin Chen, Shen Li, Yuchen Hao, Yanli Zhao, Guna Lakshminarayanan, et al. Disaggregated multi-tower: Topology-aware modeling technique for efficient large scale recommendation. *Proceedings of Machine Learning and Systems*, 6:266–278, 2024.

[73] Sudarsanan Rajasekaran, Manya Ghobadi, and Aditya Akella. CASSINI:network-aware job scheduling in machine learning clusters. In *21st USENIX Symposium on Networked Systems Design and Implementation (NSDI 24)*, pages 1403–1420, 2024.

[74] Sergey Legtchenko, Ioan Stefanovici, Richard Black, Antony Rowstron, Junyi Liu, Paolo Costa, Burcu Canakci, Dushyanth Narayanan, and Xingbo Wu. Managed-retention memory: A new class of memory for the ai era. *arXiv preprint arXiv:2501.09605*, 2025.

[75] Sergey Legtchenko, Ioan Stefanovici, Richard Black, Ant Rowstron, Junyi Liu, Paolo Costa, Burcu Canakci, Dushyanth Narayanan, and Xingbo Wu. Storage class memory is dead, all hail managed-retention memory: Rethinking memory for the ai era. In *The ACM SIGOPS 20th Workshop on Hot Topics in Operating Systems*. Association for Computing Machinery, ACM, May 2025.

[76] Qiang Zou, Yuhui Deng, Yifeng Zhu, Yi Zhou, Jianghe Cai, and Shuibing He. Dissecting i/o burstiness in machine learning cloud platform: A case study on alibaba's mlaas. *MSST*, 2024.

[77] Artjom Joosen, Ahmed Hassan, Martin Asenov, Rajkarn Singh, Luke Darlow, Jianfeng Wang, and Adam Barker. How does it function? characterizing long-term trends in production serverless workloads. In *Proceedings of the 2023 ACM Symposium on Cloud Computing, SoCC '23*, page 443–458, New York, NY, USA, 2023. Association for Computing Machinery.

[78] Norm Jouppi, George Kurian, Sheng Li, Peter Ma, Rahul Nagarajan, Lifeng Nai, Nishant Patil, Suvinay Subramanian, Andy Swing, Brian Towles, et al. Tpu v4: An optically reconfigurable supercomputer for machine learning with hardware support for embeddings. In *Proceedings of the 50th annual international symposium on computer architecture*, pages 1–14, 2023.

[79] Yazhou Zu, Alireza Ghaffarkhah, Hoang-Vu Dang, Brian Towles, Steven Hand, Safeen Huda, Adekunle Bello, Alexander Kolbasov, Arash Rezaei, Dayou Du, et al. Resiliency at scale: Managing {Google's} {TPUv4} machine learning supercomputer. In *21st USENIX Symposium on Networked Systems Design and Implementation (NSDI 24)*, pages 761–774, 2024.

[80] Pratyush Patel, Esha Choukse, Chaojie Zhang, Íñigo Goiri, Brijesh Warrier, Nithish Mahalingam, and Ricardo Bianchini. Characterizing power management opportunities for llms in the cloud. In *Proceedings of the 29th ACM International Conference on Architectural Support for Programming Languages and Operating Systems, Volume 3, ASPLOS '24*, page 207–222, New York, NY, USA, 2024. Association for Computing Machinery.

[81] nstat(8) — network statistics tool. <https://linux.die.net/man/8/nstat>. Accessed May 2025.

[82] ss(8) — socket statistics. <https://man7.org/linux/man-pages/man8/ss.8.html>. Accessed May 2025.

A System Metrics Collection

We deploy lightweight Bash agents on each node, configured for infrastructure-specific paths and millisecond-level sampling intervals. All metrics are timestamped and logged to dedicated files for synchronized post-processing.

We use *perf stat* [13] to collect hardware performance counters for the CPU and memory subsystems. In addition to general CPU events, we select platform-specific metrics: on Intel CPUs, we monitor memory-related events (e.g., *cycle_activity.stalls_l3_miss*, *mem-loads*, *mem-stores*) to capture memory hierarchy pressure, which becomes particularly pronounced when workloads involve GPU acceleration. On AMD Zen CPUs, we focus on dispatch and load-store events (e.g., *ls_dc_accesses*, *ls_dispatch.store_dispatch*, *ls_dispatch.l0_dispatch*) that reflect pipeline utilization and LS-unit activity. We monitor processor power draw and operating frequency using *turbostat*. We also extract per-core time-state counters (e.g., *user*, *system*, *idle*) from */proc/stat* and memory statistics (e.g., *MemTotal*, *MemAvailable*) from */proc/meminfo*, sampled periodically.

We use *nvidia-smi* [34] to gather GPU metrics including utilization, memory usage, power draw, ECC error rates, encoder activity, and clock frequencies. We collect volatile and aggregate ECC error metrics across major memory regions.

Network statistics are collected from multiple sources: interface-level counters from */proc/net/dev* [33], TCP retransmission counts from *nstat* [81], protocol-level metrics from *ss* [82], and InfiniBand link patterns inferred via IP mapping.

We extract I/O statistics from */proc/diskstats* [33], including read/write operations, sectors transferred, and cumulative I/O wait times. Device names are automatically inferred based on the node type.

B Reanalyzed Metrics Construction

Reveal curates a set of derived metrics. These include utilization indicators (CPU, memory, network), first-order derivatives of cumulative counters (e.g., network throughput, disk I/O), and architecture-level signals extracted from hardware performance counters.

We focus on metrics that capture execution throughput (e.g., instructions-per-cycle (IPC)), control flow irregularities (e.g., branch mispredictions), memory hierarchy behavior (e.g., cache miss and L3 stall ratios), and subsystem pressure (e.g., occupancy under contention). These indicators offer interpretable, low-level insights into potential anomalies and bottlenecks, and are derived through a lightweight post-processing step.

The combined set of raw and derived metrics forms a high-dimensional, temporally structured representation of workload behavior across execution phases and hardware subsystems. This representation underpins our downstream feature extraction and anomaly analysis pipeline.

C Example Anomaly Report

Table 4 shows a sample anomaly report automatically generated by our framework. It retains raw detector outputs and augments them with concise, evidence-based claims.

D Software Environment

The containerized environments for both GPU- and CPU-centric clusters were built with Conda and executed via AppTainer (Singularity v3.11.0 on GPU clusters, v1.2.2 on CPU clusters). The stack was designed to support distributed ML training and system-level telemetry across heterogeneous infrastructures.

The software stack included CUDA 12.4 (with cuDNN, cuBLAS, cuFFT, cuRAND, cuSOLVER, cuSPARSE), PyTorch 2.6.0 with torchvision and torchaudio, and math/data libraries such as MKL, NumPy, SciPy, SymPy, pandas, and PyArrow. Optimization and training utilities (bitsandbytes, FlashAttention, Triton, PEFT, TRL) were integrated alongside visualization (matplotlib, seaborn), CV toolkits (OpenCV, Ultralytics), and system utilities (accelerate, PyYAML, requests, protobuf, rich). All packages were sourced from the *conda-forge*, *pytorch*, and *nvidia* channels, and the complete pinned environment is reproducible from the original YAML specification.

E Workload Configuration Details

Reveal evaluated ML workloads spanning NLP and CV. Table 5 summarizes the models, associated tasks, and corresponding datasets.

Most workloads are executed repeatedly on two distinct platforms to capture runtime variability across environments. As shown in Table 6, training parameters for general-purpose models are standardized across tasks, with 5 training epochs used to ensure comparability. The choice of optimizer depends on the task and model complexity: AdamW is employed for NLP tasks, whereas either SGD or Adam is used for CV workloads. Hyperparameters such as learning rate and momentum are tuned to maximize training effectiveness for each model-task pair. As shown in Table 7, the LLMs evaluated, DeepSeek, LLaMA, and Mistral, are fine-tuned under a standardized setup to ensure consistency and support fair cross-model comparisons.

All models are fine-tuned using LoRA-based parameter-efficient techniques, with unified low-rank settings and 4-bit quantization to enable training under constrained computational budgets. Key hyperparameters: batch size, gradient accumulation steps, and learning rate, are kept consistent across all LLMs. The *paged_adamw_8bit* optimizer is used together with Fully Sharded Data Parallel (FSDP), employing hybrid sharding and mixed-precision training. Unless

Table 4: Automatically generated anomaly report. We preserve raw detector outputs (window, methods, and `mainreasons`) and add concise, evidence-based claims.

Window (ID / Timestamp)	Method(s)	Subsystem	Mainreasons (Metric-Temporal Feature)	Claim
37 / 10:32:05	Z	CPU	Busy%. __value__variance	CPU busy percentage shows different within-window variance relative to baseline.
38 / 10:32:06	IF, MAHA	CPU	Bzy_MHz. __value__autocorrelation_lag_1	CPU operating frequency exhibits different lag-1 autocorrelation with the baseline.
400 / 10:38:14	MAHA	Storage	sectors_read. __value__maximum	Disk read sectors' maximum exceeds the baseline reference, reflecting a single-window spike in read volume.
402 / 10:38:16	Z, IF	Network	NetworkUtilization. __value__standard_deviation	Network utilization shows a different standard deviation versus baseline.

Table 5: Summary of evaluated models, tasks, and datasets.

Model	Task	Dataset
Deepseek-R1 -Distill-Qwen-7B/1.5B	Text Cls.	GLUE/SST2
Meta-LLaMA -3-8B/-3.2-1B	Text Cls.	GLUE/SST2
Mistral-7B-v0.3	Text Cls.	GLUE/SST2
BART-base/large	Table QA	WIKISQL
BERT-base/large/ DistilBERT	Text Cls.	GLUE/SST2
ResNet18/50	Img. Seg.	PASCAL VOC12
VGG16/19	Img. Cls. Seg.	MNIST, CIFAR10/100
ViT-B16/L16	Img. Cls. Seg.	PASCAL VOC12
	Img. Cls.	MNIST, CIFAR10/100

Table 6: Configuration for General-Purpose Models.

ML Workloads	Optimizer	BS
BART for Table QA and Text Cls.	AdamW ¹ , lr ⁴ =5e-5	16
BERT for Text Cls.	AdamW ¹ , lr ⁴ =5e-5	64
Resnet and VGG for Img Cls.	SGD ² , lr ⁴ =1e-3	64
Resnet and VGG for Img Seg., ViT for Img Cls. and Seg.	Adam ³ , lr ⁴ =1e-3	64

[1]AdamW: Adam³ with weight decay. [2]SGD: Stochastic Gradient Descent. [3]Adam: Adaptive Moment Estimation. [4]lr: Learning rate.

Table 7: Unified configuration for LLMs on text Cls.

Params	DeepSeek	LLaMA	Mistral
Model	Deepseek-R1- Distill-Qwen-7B	Meta-Llama- 3-8B	Mistral-7B- v0.3
Shared Configuration			
LoRA ¹	$r = 4$, $lora_alpha = 32$, $dropout = 0.05$, target modules = q_proj, v_proj		
Quant ²	4-bit (NF4), double quantization enabled, float16 compute and storage		
Train		2	
BS ³		1	
Eval		8	
BS ⁴		5	
Grad		2e-4	
Acc ⁵		paged_adamw_8bit	
Epochs		2e-4	
Optimizer		Hybrid shard, auto wrapping, mixed precision enabled	
LR ⁶		Greedy decoding(0°C), $max_new_tokens=1$, prompt: "Text: <input> Sentiment:"; left-padded, pad = EOS, 512 max length	
FSDP ⁷			
Inference			

[1]Low-Rank Adaptation Configuration. [2]Quantization. [3]Training Batch Size. [4]Evaluation Batch Size. [5]Gradient Accumulation Steps. [6]Learning Rate. [7]Fully Sharded Data Parallel.

otherwise noted, all experiments involve fine-tuning (rather than pre-training) due to infrastructure constraints. Specifically, LLMs are fine-tuned using 2% of the GLUE/SST-2 dataset. For inference, greedy decoding with temperature 0.0 and $max_new_tokens=1$ is employed to extract sentiment labels. Inputs follow a fixed prompt template: *Text: <input_sentence> Sentiment:* To align with training, input

sequences are left-padded, use EOS as the padding token, and are truncated at 512 tokens. Output predictions are post-processed using substring matching (e.g., any output containing “positive” is labeled as such).

To support CPU-only environments where 7B+ LLMs cannot be loaded due to limited memory resources (e.g., 2 cores, 4 threads, 20 GB per node), smaller variants, DeepSeek-R1-Distill-Qwen-1.5B and LLaMA-3.2-1B, are fine-tuned and evaluated using the same setup described in Table 7. These models follow the same LoRA configuration, quantization scheme, optimizer, and training parameters as their larger counterparts. Both fine-tuning and inference are performed on the SST-2 sentiment classification task. Logging, data pre-processing, and prompt formatting are kept consistent across both deployment environments.

F What Low-Level Metrics Matter?

Table 8 presents representative low-level metrics collected by our monitoring framework and highlights the additional insights they offer beyond traditional utilization counters.

Table 8: Representative low-level metrics & their diagnostic value.

Subsystem	Low-Level Metrics	Insights Beyond Util.
CPU	<i>Bzy_MHz</i> , <i>stalls_l3_miss</i> <i>PkgWatt</i> , <i>CoreTmp</i> , <i>Pkg%pc6</i>	Detects memory stalls despite high core usage. Reveals throttling or power-state transitions not visible from CPU utilization.
GPU	<i>power_draw</i> , <i>temperature_gpu</i> , <i>ecc_errors</i>	Shows low compute saturation despite high utilization (e.g., due to ECC faults or memory contention).
Memory	<i>Mem_loads</i> , <i>Mem_stores</i> , <i>latency_gt_256</i>	Highlights cache misses and memory latency under low memory usage.
Network	<i>TcpRetransSegs</i>	Exposes packet loss and retransmissions despite stable bandwidth usage.
Storage	<i>time_spent_reading</i> , <i>sectors_read</i>	Reveals I/O delays and access skew under low throughput.

G Open Dataset and Toolkit

To support reproducible research and enable further study of system-level ML workload behavior, we release both our

curated telemetry dataset and the full profiling toolkit as open-source resources.

G.1 Curated Telemetry Dataset

Our dataset comprises host-level time-series metrics collected from multiple distinct ML applications, with each kind of workload executed 10 times under controlled conditions in both deployment environments. The dataset includes:

Raw Metrics: Over 700 system-level metrics per node per run, sampled at 100Hz, covering CPU, GPU, memory, network, and storage subsystems.

Filtered Metrics: A refined subset of 150 stable and discriminative metrics selected through our pipeline.

Annotated Windows: Sliding windows with extracted features and corresponding anomaly scores from Z-score, Mahalanobis distance, and Isolation Forest.

Metadata: Workload type, task, environment (cloud/HPC), and model architecture information.

All data are stored in compressed text format with accompanying schema files for easy parsing. The dataset is hosted on Hugging Face at <https://huggingface.co/datasets/susetchen/RevealTelemetryDatasetforMLInfraProfilingAnomalyDetection>.

G.2 Profiling Toolkit

We also release the full profiling toolkit used to collect and process telemetry, designed for extensibility and low overhead. The toolkit includes:

Modular Collectors: Shell-based agents for capturing metrics via *perf*, *turbostat*, *nvidia-smi*, *procfs*, and *nstat*, with configurable sampling intervals.

Filtering and Feature Extraction Modules: Python scripts for metric selection (CV, variance, correlation, DTW, ANOVA) and feature computation using *tsfresh*.

Anomaly Detection Engine: Implementations of Z-score, Mahalanobis, and Isolation Forest applied to time-series windows.

Visualization Utilities: Tools for plotting subsystem-specific anomalies, UMAP/t-SNE projections, and CDFs of key resource usage metrics.

The toolkit is platform-agnostic, lightweight, and can be deployed in both containerized and bare-metal environments. It is intended for researchers, platform engineers, and practitioners seeking visibility into workload-level system behavior without requiring privileged access.